CLM-P784

CLM-P784

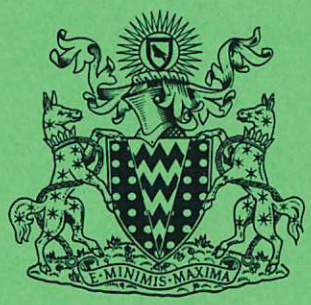

UKAEA

Preprint

THE EFFECT OF ASYMMETRIC CURRENT-SUPPORTING ELECTRON VELOCITY DISTRIBUTIONS ON SECOND HARMONIC ELECTRON CYCLOTRON RESONANCE HEATING: A RAY-TRACING TREATMENT FOR THE COMPASS TOKAMAK

R. O. DENDY
A. MONTES
J. P. LEITE

CULHAM LABORATORY
Abingdon, Oxfordshire

1986

CLM-P784

THE EFFECT OF ASSYMMETRIC CURRENT-SUPPORTING ELECTRON VELOCITY DISTRIBUTIONS ON SECOND HARMONIC ELECTRON CYCLOTRON RESONANCE HEATING: A RAY-TRACING TREATMENT FOR THE COMPASS TOKAMAK

R.O. Dendy

Culham Laboratory, Abingdon, Oxon, OX14 3DB, UK

(Euratom/UKAEA Fusion Association)

A. Montes and J.P. Leite

Instituto de Pesquisas Espaciais, C.P. 515, 12 200 São José dos Campos, S.P., BRAZIL

Abstract

A limited asymmetric distortion of the distribution of electron velocities parallel to the magnetic field, sufficient to support the plasma current, is considered. Its effects on second harmonic electron cyclotron absorption of the extraordinary mode propagating away from normal incidence are quantified using a fully three-dimensional ray-tracing code. Significant deviations from the zero current power deposition profiles occur, both in real space and in velocity space. At higher densities, the effects of the extraordinary mode cutoff are softened. These considerations should be taken into account in future studies of temperature and current profile modification using second harmonic electron cyclotron absorption on COMPASS.

(Submitted for publication in Physics of Fluids)

52.50.Gj 52.40.Db 52.25.Mq 52.55.Fa

July 1986

I. INTRODUCTION

In this paper, we use a ray-tracing code together with a non-Maxwellian electron velocity distribution to address the following question. What is the effect on second harmonic electron cyclotron absorption of a parallel electron velocity distribution which has an asymmetry sufficient to support a realistic tokamak plasma current? Localised electron cyclotron resonance heating (ECRH) and current drive[1] are being considered as a means of temperature and current profile modification and control.[2-7] Accordingly, it is of interest to obtain a quantitative description of the consequences of realistic asymmetry in the parallel electron velocity distribution for the power deposition profile in velocity space and in real space.

Second harmonic heating is of general interest firstly because it enables existing gyrotron technology to be employed in conjunction with relatively low magnetic fields ($B \sim 1T$) for studies of tokamak plasmas at high beta; and secondly because an outside launch position can be used - advantageously from an engineering point of view - without the low-density extraordinary mode cutoff interposing between the source and the resonance. We have applied our analysis and ray-tracing code to the COMPASS tokamak[8] (major radius R_o = 56 cm, minor radius a = 22 cm) under construction at Culham Laboratory, where ECRH will take place at the second harmonic using 60 GHz gyrotrons. At typical temperatures and densities ($T_e(0) \simeq 1$ keV, $n_e(0) \simeq 10^{13}cm^{-3}$), the plasma current $I_p \gtrsim 250$

kA may be supported by a limited asymmetric distortion of the bulk Maxwellian electron velocity distribution, rather than by an extended superthermal tail of the kind considered in our ray-tracing treatment in another context of ECRH at the fundamental resonance.[9] Such electron distributions may be represented in the form

$$f(v_\perp, v_\parallel) = (1 - \mu) f_B(v_\perp, v_\parallel) + \mu f_T(v_\perp, v_\parallel) \tag{1}$$

$$f_B(v_\perp, v_\parallel) = \frac{\pi^{-3/2}}{v_B^3} e^{-v_\perp^2/v_B^2} e^{-v_\parallel^2/v_B^2} \tag{2}$$

$$f_T(v_\perp, v_\parallel) = \frac{\pi^{-3/2}}{v_T^3} e^{-v_\perp^2/v_T^2} e^{-(v_\parallel - v_o)^2/v_T^2} \tag{3}$$

This distribution is normalised to unity. The associated total plasma current is

$$I_p = e \int_o^a 2\pi r dr \int d^3v \, n_e(r) v_\parallel f(v_\perp, v_\parallel)$$

$$= \mu \left(\frac{v_o}{v_B}\right) \left(\frac{n_e(o)}{10^{13}\ \mathrm{cm}^{-3}}\right) \left(\frac{T_e(o)}{1\ \mathrm{keV}}\right)^{1/2} \left(\frac{a}{10\ \mathrm{cm}}\right)^2 480\ \mathrm{kA} \tag{4}$$

where we have assumed a parabolic electron density profile $n_e(r) = n_e(0)(1 - r^2/a^2)$. The plasma parameters stated above, together with Eq.(4), yield the constraint

$$\mu(v_o/v_B) \simeq 0.1 \tag{5}$$

on the asymmetry parameters. In our numerical examples, we have chosen $\mu \simeq 0.1$ and $v_o \simeq v_B$, see Fig. 1.

In order to describe wave propagation and absorption in the ray-tracing method, it is necessary to calculate the warm-plasma dielectric tensor for the distribution of Eqs.(1)-(3), and then the localised dispersion relation. These calculations are carried out in the next Section, applying a nonrelativistic approximation which we discuss in Section III. We note that ideally, for maximum realism and flexibility, a fully relativistic ray-tracing treatment of second harmonic absorption for non-Maxwellian distributions is required. The first step in this direction has already been taken,[1] in the form of a relativistic Maxwellian treatment. Here, we present a nonrelativistic but also non-Maxwellian treatment. A ray-tracing treatment that is both relativistic and non-Maxwellian remains a topic for further research. We present the numerical results in Section IV, and our conclusions in Section V.

II. DERIVATION OF THE BASIC EQUATIONS

We are concerned with second harmonic electron cyclotron resonance:

$$\omega = 2\Omega_e(0) \tag{6}$$

where ω denotes the fixed frequency of the applied radiation and $\Omega_e(0)$ denotes the central electron cyclotron frequency. Poles in the dielectric tensor elements, giving rise to absorption, arise from the resonances $\zeta_2 = 0$ and $\eta_2 = 0$, where

$$\zeta_n = \frac{\omega - n\Omega_e}{k_\parallel v_B}, \qquad \eta_n = \frac{\omega - k_\parallel v_o - n\Omega_e}{k_\parallel v_B} \tag{7}$$

Here $k_\parallel$ is the component of the wavenumber $\underline{k}$ parallel to the magnetic field. In the nonrelativistic approximation, to be discussed in Section III, the dielectric tensor which includes these resonances can be calculated from Eqs.(1)-(3) and the general integral expressions.[11] Using a first-order finite Larmor radius expansion, we obtain

$$\underline{\underline{\varepsilon}} = \begin{bmatrix} \varepsilon_1 + W_{xx} & i(\varepsilon_2 - W_{xx}) & W_{xz} \\ -i(\varepsilon_2 - W_{xx}) & \varepsilon_1 + W_{xx} & iW_{xz} \\ W_{xz} & -iW_{xz} & \varepsilon_3 + W_{zz} \end{bmatrix} \tag{8}$$

where

$$\varepsilon_1 = 1 - \frac{X}{1 - Y^2}, \qquad \varepsilon_2 = \frac{XY}{1 - Y^2}, \qquad \varepsilon_3 = 1 - X \tag{9}$$

are the usual cold-plasma expressions, taking

$$X = (\omega_p/\omega)^2, \qquad Y = (\Omega_e/\omega) \tag{10}$$

In Eq.(10), ω_p denotes the electron plasma frequency. The warm-plasma terms in Eq.(8) are given by

$$W_{xx} = \frac{X\beta}{2}\left[\zeta_o Z(\zeta_2) + \mu\left(\frac{v_T}{v_B}\right)^2 \eta_o Z(\eta_2)\right] \tag{11}$$

$$W_{xz} = \left(\frac{\beta}{2}\right)^{1/2} \zeta_2 W_{xx} , \quad W_{zz} = \frac{\beta}{2}\zeta_2^2 W_{xx} \tag{12}$$

Here Z denotes the plasma dispersion function,[12] and

$$\beta = \left(k_\perp^2 v_B^2/2\Omega_e^2\right) \tag{13}$$

We shall only be concerned with the imaginary terms arising from the warm-plasma correction, so that in Eq.(11) we have

$$W_{xx} = \frac{i\pi^{1/2} X\beta}{2}\left[\zeta_o e^{-\zeta_2^2} + \mu\left(\frac{v_T}{v_B}\right)^2 \eta_o\, e^{-\eta_2^2}\right] \tag{14}$$

Maxwell's equations take the general form $\underline{N} \times (\underline{N} \times \underline{E}) + \underline{\underline{\varepsilon}}.\underline{E} = 0$, where $\underline{N} = c\underline{k}/\omega$. We define a propagation angle θ such that $N_\parallel = N\cos\theta$ and $N_\perp = N\sin\theta$ are the components of $\underline{N}$ parallel and perpendicular to the magnetic field. Then Maxwell's equations, together with Eqs.(8)-(14), yield the following dispersion relation for the local normal modes:

$$D^C + i\,\mathrm{Im}\,D^W = 0 \tag{15}$$

$$D^C = N^4\left[\varepsilon_1 \sin^4\theta + (\varepsilon_1 + \varepsilon_3)\sin^2\theta\cos^2\theta + \varepsilon_3\cos^4\theta\right] \tag{16}$$

$$- N^2\left[\varepsilon_1\varepsilon_3(1 + \cos^2\theta) + (\varepsilon_1^2 - \varepsilon_2^2)\sin^2\theta\right] + \varepsilon_3(\varepsilon_1^2 - \varepsilon_2^2)$$

$$\mathrm{Im}\,D^W = \frac{\pi^{1/2}\,X\,v_B^2}{4Y^2}\,\frac{B}{c^2}\,N^2\sin^2\theta\left[\zeta_o\, e^{-\zeta_2^2} + \mu\left(\frac{v_T}{v_B}\right)^2 \eta_o\, e^{-\eta_2^2}\right] \tag{17}$$

$$\times \left[F_1 + F_2\left(\frac{1}{2Y} - 1\right) + F_3\left(\frac{1}{2Y} - 1\right)^2\right]$$

$$F_1 = N^2\sin^2\theta\left[N^2 - 2(1 - X + Y)/(1 + Y)\right] - N^2(1 + \cos^2\theta)(1 - X) \tag{18}$$

$$+ 2(1 - X + Y)(1 - X)/(1 + Y)$$

$$F_2 = 2N^2\sin^2\theta\left[N^2 - (1 - X + Y)/(1 + Y)\right] \tag{19}$$

$$F_3 = N^4\sin^2\theta - N^2(\tan^2\theta + \sin^2\theta)(1 - X - Y^2)/(1 - Y^2) \tag{20}$$

$$+ \tan^2\theta\left[(1 - X)^2 - Y^2\right]/(1 - Y^2)$$

The imaginary part N_i of the refractive index is given to good approximation by[13]

$$N_i = \frac{-\,\mathrm{Im}\, D^W(N,\Theta)}{\frac{N_\parallel}{N}\frac{\partial D^C}{\partial N_\parallel} + \frac{N_\perp}{N}\frac{\partial D^C}{\partial N_\perp}} \qquad (21)$$

where $N_\perp$ and $N_\parallel$ satisfy $D^C(N_\perp, N_\parallel) = D^C(N,\Theta) = 0$.

The results Eqs.(16)-(20) form the basis of our ray-tracing treatment of second harmonic cyclotron absorption by asymmetric current-supporting electron velocity distributions in the COMPASS tokamak. We have amended the original Culham ray-tracing code[14] accordingly, and in Section IV the numerical results will be given.

III. NONRELATIVISTIC APROXIMATION

In general, the quantity Ω_e in Eq.(7) depends on electron velocity through the relativistic variation of mass, as well as on spatial position. We have neglected this relativistic correction in the analysis in Section II; its inclusion would have complicated the analysis substantially. There is no general theory for the validity of the nonrelativistic approximation for cyclotron absorption in non-Maxwellian plasmas. We therefore employ as guidelines the criteria when the distribution is Maxwellian:[15-17]

$$N_\parallel^2 >> \mathrm{Max}\left\{(v_{\mathrm{thermal}}/c)^2\,,\ \ (2/n)\left|(\omega - n\Omega_e)/\Omega_e\right|\right\} \qquad (22)$$

For a fusion plasma with $v_{\mathrm{thermal}} << c$, the second condition in Eq.(22) is the more restrictive. The variation of Ω_e with the distance R from

the tokamak axis of symmetry is $\Omega_e \sim \frac{1}{R}$, and for second harmonic $(n = 2)$ resonance at the plasma centre, $\omega = 2\Omega_e(R_o)$. Then by Eq.(22), the nonrelativistic approximation remains valid for given $N_\parallel$ so long as the value of R where absorption occurs satisfies

$$|(R - R_o)/R_o| \ll N_\parallel^2/2 \tag{23}$$

In the numerical results presented below, the launch angle has been set at 30° from the perpendicular, so that $N_\parallel = 0.5$ and satisfies Eq.(23). This constraint on Θ does not restrict us unduly, since for current drive purposes, interest is concentrated on the extraordinary mode launched from the low-field side and propagating away from the perpendicular.

Recently, Bornatici and Ruffina[18] have studied numerically the difference between the fully relativistic and nonrelativistic approaches to second harmonic electron cyclotron absorption for a Maxwellian plasma in slab geometry. These calculations provide a useful extension to the analytical arguments introduced above. The relativistic corrections tend to shift the absorption profile towards the high-field side of the plasma, and the correction is proportionately largest towards the edge of the absorption profile. These effects become more pronounced as the launch angle tends to the perpendicular. For the launch angle of 30° that we consider, however, the relativistic correction to the nonrelativistic treatment is typically ten per cent or less. We conclude that the nonrelativistic approximation used in the analysis in Section II is valid in the context where we shall employ it.

IV. RESULTS

A poloidal projection of the rays for second harmonic electron cyclotron resonance heating with low field side launch on COMPASS is shown in Fig. 2. Each cross on a ray marks a five per cent decrement in power due to absorption. The plasma parameters are $n_e(0) = 10^{13}$ cm^{-3}, $T_e(0) = 1$ keV, and the toroidal and poloidal magnetic fields are 1.07T and 0.22T respectively. The electron velocity distribution is of the form shown in Fig. 1, which is represented by Eqs.(1)-(3) with $\mu = 0.15$, $v_o = 0.7\ v_B$, and $v_T = v_B$; see also Eq.(5). The role of the asymmetry associated with the current can be seen in Figs. 3-5, where the dashed profiles correspond to the zero-current case $\mu = v_o = 0$.

In Fig. 3, the total power absorbed over a toroidal surface at a given distance from the magnetic axis is plotted as a function of distance from the magnetic axis. The effect of the current is slightly to broaden the spatial absorption profile and shift it in the direction of greater distances from the magnetic axis. For the surface at $r = 4$cm, the power absorbed with the current-carrying distribution exceeds that with a zero-current symmetric distribution by 25%. In Fig. 4, the power deposition profile in $v_\parallel$ - space is shown. The profile is shifted in the direction of greater $v_\parallel$ for the current-carrying distribution. The corresponding integrated power deposition is shown in Fig. 5, where the height of the graph at a given value of $v_\parallel$ is equal to the fraction of the incident power absorbed by all electrons with $v_\parallel$ exceeding the given value. From these Figures, it can be seen that the current-carrying plasma is a better absorber of radiation. It absorbs 86% of the incident power, compared to 81% in the symmetric case. For the purpose of current

drive, it is interesting to note that electrons with $v_{\parallel} > v_B$ absorb 24% of the incident power in the current-carrying case, compared to only 15% in the zero-current case. Similar effects have been found throughout the range $0.067 < \mu < 0.15$, $0.7\ v_B < v_o < 1.5\ v_B$, subject to Eq.(5). We believe that these are significant changes. They will need to be taken into account in, for example, calculating the sustainment by electron cyclotron waves of initially inductive current in COMPASS, and in any fine control of the current profile by localised ECRH.[1-7]

In denser plasmas, the low-density extraordinary mode cutoff may prevent waves from reaching the second harmonic cyclotron resonance in the centre of the plasma. This is shown in Fig. 6, where $n_e(0) = 1.5 \times 10^{13}\ cm^{-3}$, $\mu = 0.067$, $v_o = 1.5\ v_B$ and $v_T = v_B$. In this case, wave absorption can still occur: the Doppler shift $\omega > \omega - k_{\parallel} v_{\parallel}$ enables electrons on the low field side to resonate with incident waves. The sensitivity of this effect to the nature of the distribution function can be seen in Figs. 7-9, which are the counterparts to Figs. 3-5. Here, $\mu = 0.067$, $v_o = 1.5\ v_B$, and $v_T = v_B$. The integrated absorption for this current-carrying plasma is 17%, double that of the zero-current plasma shown by the dashed line. Absorption is shifted spatially to the low-field side for the current-carrying plasma, and in velocity space to higher $v_{\parallel}$. The latter result is of interest for current drive, since absorption takes place only on electrons with $v_{\parallel} > 0$, which is advantageous. It is clear that the density limit on extraordinary mode second harmonic electron cyclotron resonance heating is somewhat softened when allowance is made for the fact that the electron velocity distribution supports the plasma current.

V. CONCLUSIONS

An accurate ray-tracing code in realistic toroidal geometry has been employed to study the second harmonic electron cyclotron resonance heating of electron velocity distributions which possess an asymmetry sufficient to support the tokamak plasma current. The distributions chosen have the form shown in Fig.1, which is represented by Eqs.(1)-(3) subject to the constraint of Eq.(5). Plasma geometry and parameters appropriate to the COMPASS tokamak[8] have been used throughout. Treatment has been restricted to the extraordinary mode away from normal incidence in the nonrelativistic approximation. The asymmetry in the parallel electron velocity distribution gives rise to significant alterations in the power deposition profile, both in real space and particularly in velocity space. These effects will need to be taken into account in studies of electron cyclotron current sustainment and of temperature profile control. At higher plasma densities, the role of the extraordinary mode cutoff is softened when an asymmetric current-carrying electron velocity distribution is considered. This study has provided quantitative indications of the magnitude of these effects, which should be included in future self-consistent treatments of these topics. In addition, it motivates the longer-term development of ray-tracing codes which can both give a relativistic description[10] and deal with non-Maxwellian velocity distributions in this context.

ACKNOWLEDGEMENT

We are grateful to M.Bornatici and U.Ruffina for making available to us the calculations referred to at the end of Section III.

REFERENCES

1 N.J. Fisch and A.H. Boozer, Phys. Rev. Lett. 45, 720 (1980).

2 V. Chan and G. Guest, Nucl. Fusion 22, 272 (1982).

3 A.H. Reiman, Phys. Fluids 26, 1338 (1983).

4 T-10 Group, A.P. Andreev, B.V. Kuteev, S.V. Skobolnikov, A.P. Umov, V.G. Usov, V.A. Flyagin, H.W. Piekaar, R.M.J. Sillen, Th. Oyevaar, and A. Cavallo, Proc. 11th Eur. Conf. on Controlled Fusion and Plasma Phys., Aachen (European Physical Society, 1983), Part I, p.289.

5 P.H. Rebut and M. Hugon, Proc. 10th Int. Conf. on Plasma Phys. and Controlled Fusion, London (IAEA, Vienna, 1985), Vol.2, p.197.

6 D.W. Ignat, P.H. Rutherford, and H. Hsuan, Proc. Course and Workshop on Applications of RF Waves to Tokamak Plasmas, Varenna (Monotypia Franchi, Perugia, 1985), Vol.II, p.525.

7 R.O. Dendy, Plasma Phys. 27, 1243 (1985).

8 A.C. Riviere, M.W. Alcock, A.N. Dellis, M. Hughes, D.C. Robinson, and T.N. Todd, Proc. Course and Workshop on Applications of RF Waves to Tokamak Plasmas, Varenna (Monotypia Franchi, Perugia, 1985), Vol.II, p.797.

[9] A. Montes and R.O. Dendy, Phys. Fluids 29, to be published (1986).

[10] B. Hui, K.R. Chu, E. Ott, and T. Antonsen, Phys. Fluids 23, 822 (1980).

[11] N.A. Krall and A.W. Trivelpiece, Principles of Plasma Physics (McGraw-Hill, London, 1973), p.405.

[12] B.D. Fried and S.D. Conte, The Plasma Disperson Function (Academic, New York, 1961).

[13] A.I. Akhiezer, I.A. Akhiezer, R.V. Polovin, A.G. Sitenko, and K.N. Stepanov, Plasma Electrodynamics (Pergamon, Oxford, 1975), Vol.I.

[14] P.J. Fielding, private communication.

[15] I.P. Shkarofsky, Phys. Fluids 9, 561 (1966).

[16] I. Fidone, G. Granata, and R.L. Meyer, Phys. Fluids 25, 2249 (1982).

[17] M. Bornatici, R. Cano, O. De Barbieri, and F. Engelmann, Nucl. Fusion 23, 1153 (1983).

[18] M. Bornatici and U. Ruffina, private communication.

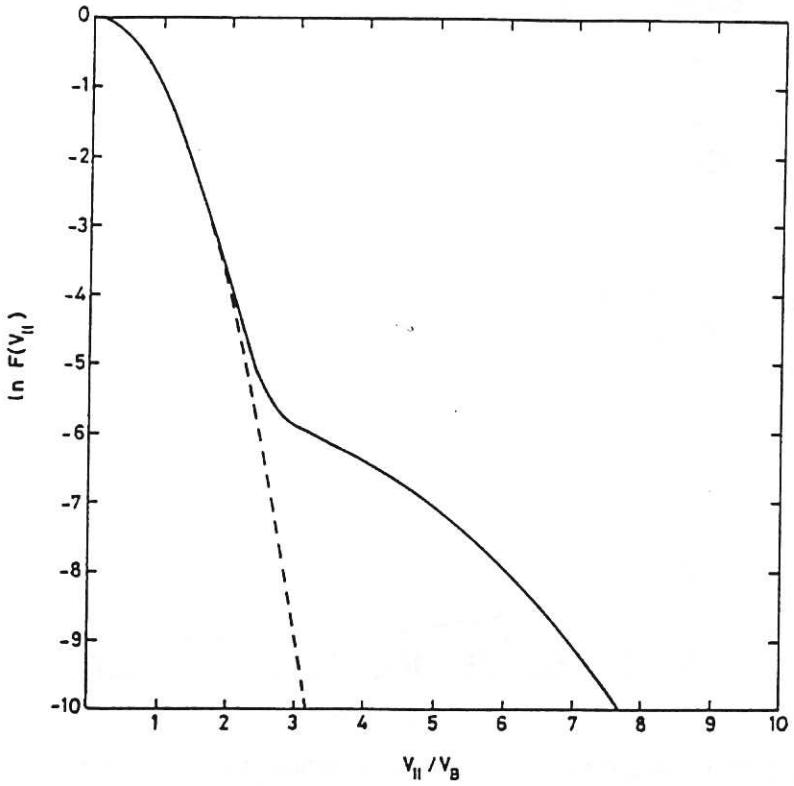

Fig. 1 Parallel electron velocity distribution for the case of Eqs.(1)-(3) with $\mu=0.15$, $v_o=0.7v_B$, $v_T=v_B$.

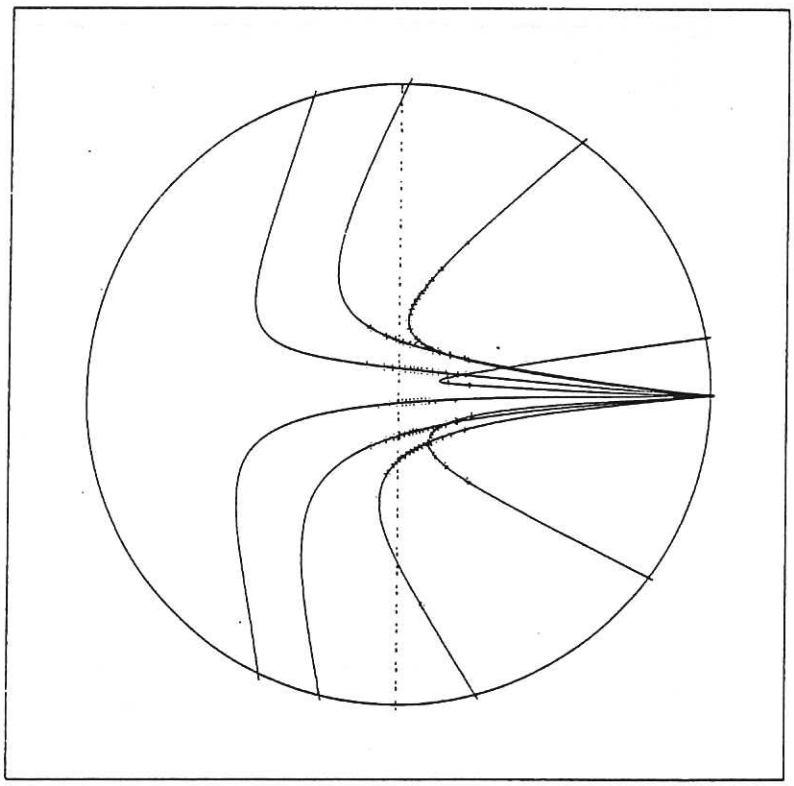

Fig. 2 Minor cross section projection of ray trajectories for the COMPASS tokamak, with the parallel electron velocity distribution of Fig. 1. Launch angle is 30° to the perpendicular. The vertical dashed line denotes the second harmonic resonance, and each cross on a ray marks a five per cent decrement in wave power. Plasma parameters are $n_e(0)=10^{13}\,\mathrm{cm}^{-3}$, $T_e(0)=1\,\mathrm{keV}$, $B_T=1.07\,\mathrm{T}$, and $B_p=0.22\,\mathrm{T}$.

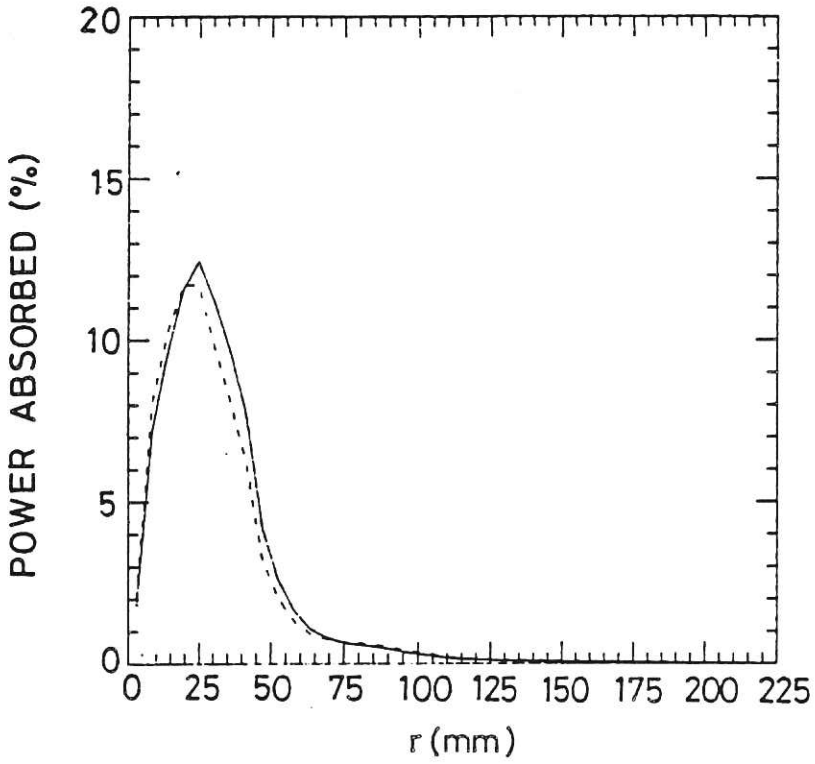

Fig. 3 Total power deposited on a toroidal surface at a given distance from the magnetic axis, as a function of that distance. Parameters as in Figs. 1 and 2. Dashed curve denotes zero-current case.

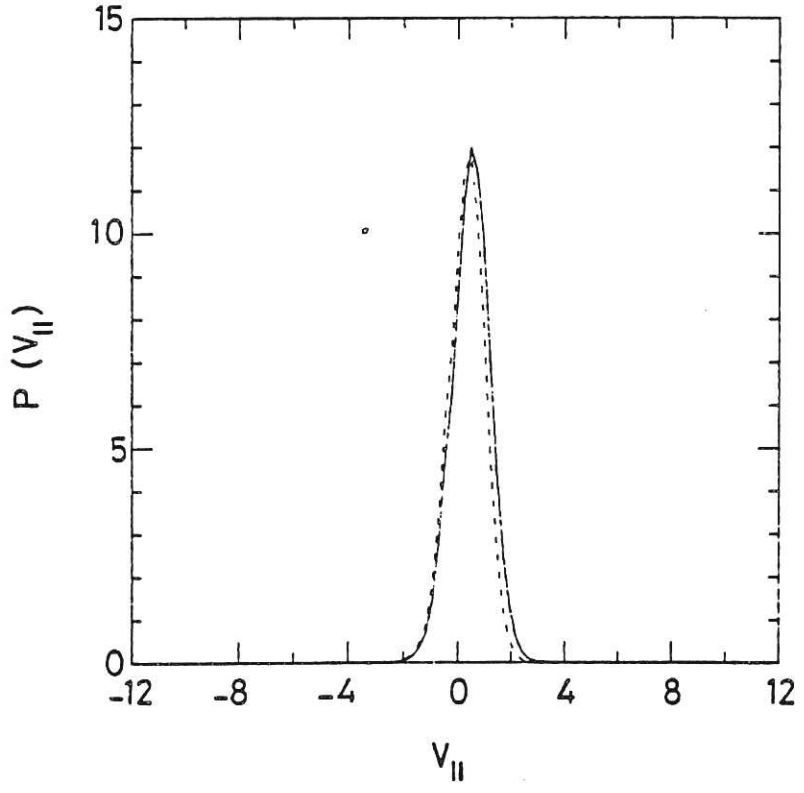

Fig. 4 Power deposition as a function of parallel electron velocity. Parameters as in Figs. 1 and 2. Dashed curve denotes zero-current case.

CLM-P784

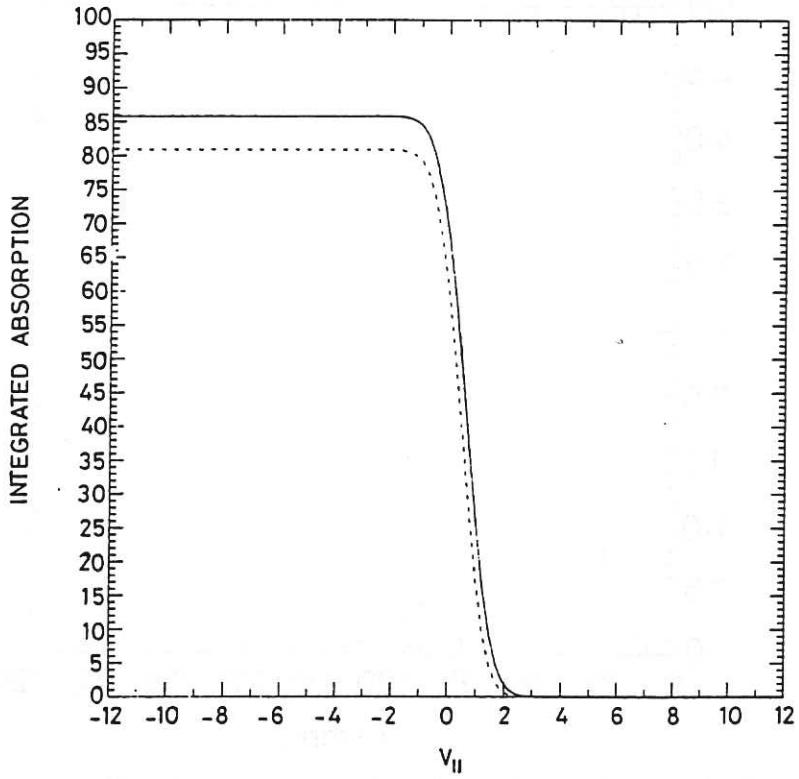

Fig. 5 Integrated power deposition as a function of parallel electron velocity. Parameters as in Figs. 1 and 2. Dashed curve denotes zero-current case.

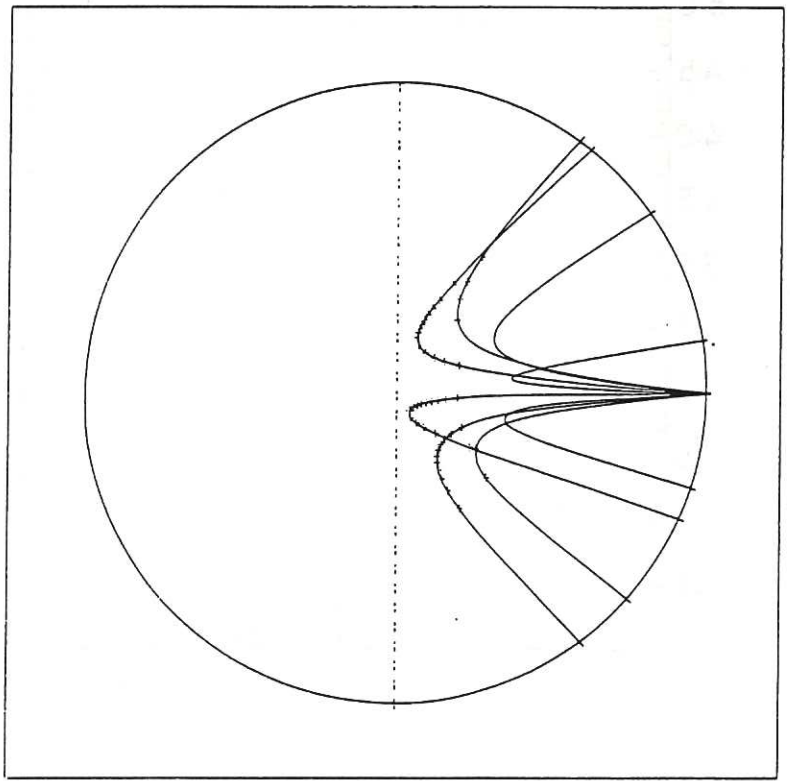

Fig. 6 As Fig. 2, for a denser plasma with $n_e(0)=1.5\times10^{13}\,\mathrm{cm}^{-3}$, which has the extraordinary mode cutoff between launch position and second harmonic resonance. Here $\mu=0.067$, $v_o=1.5v_B$, and $v_T=v_B$, and launch angle is 30° to the perpendicular.

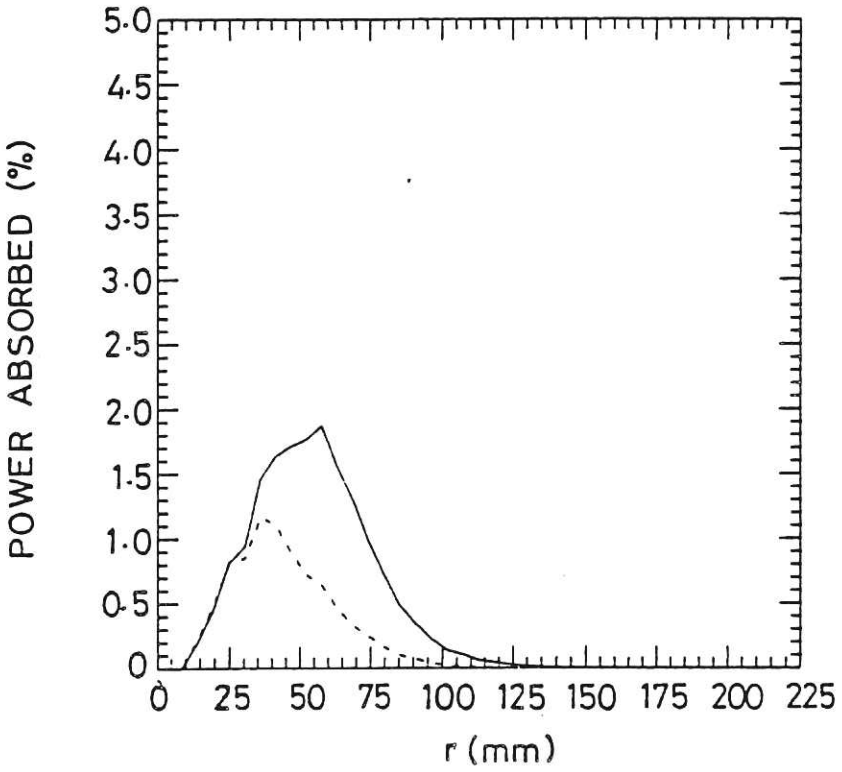

Fig. 7 Total power deposited on a toroidal surface at a given distance from the magnetic axis, as a function of that distance for parameters of Fig. 6.

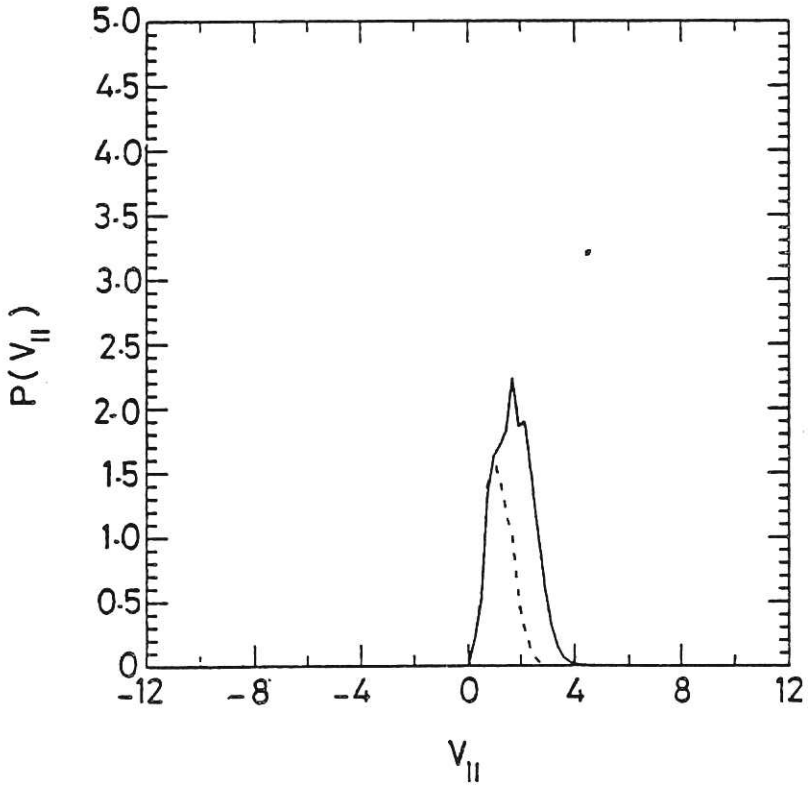

Fig. 8 Power deposition as a function of parallel electron velocity, for parameters of Fig. 6.

CLM-P784

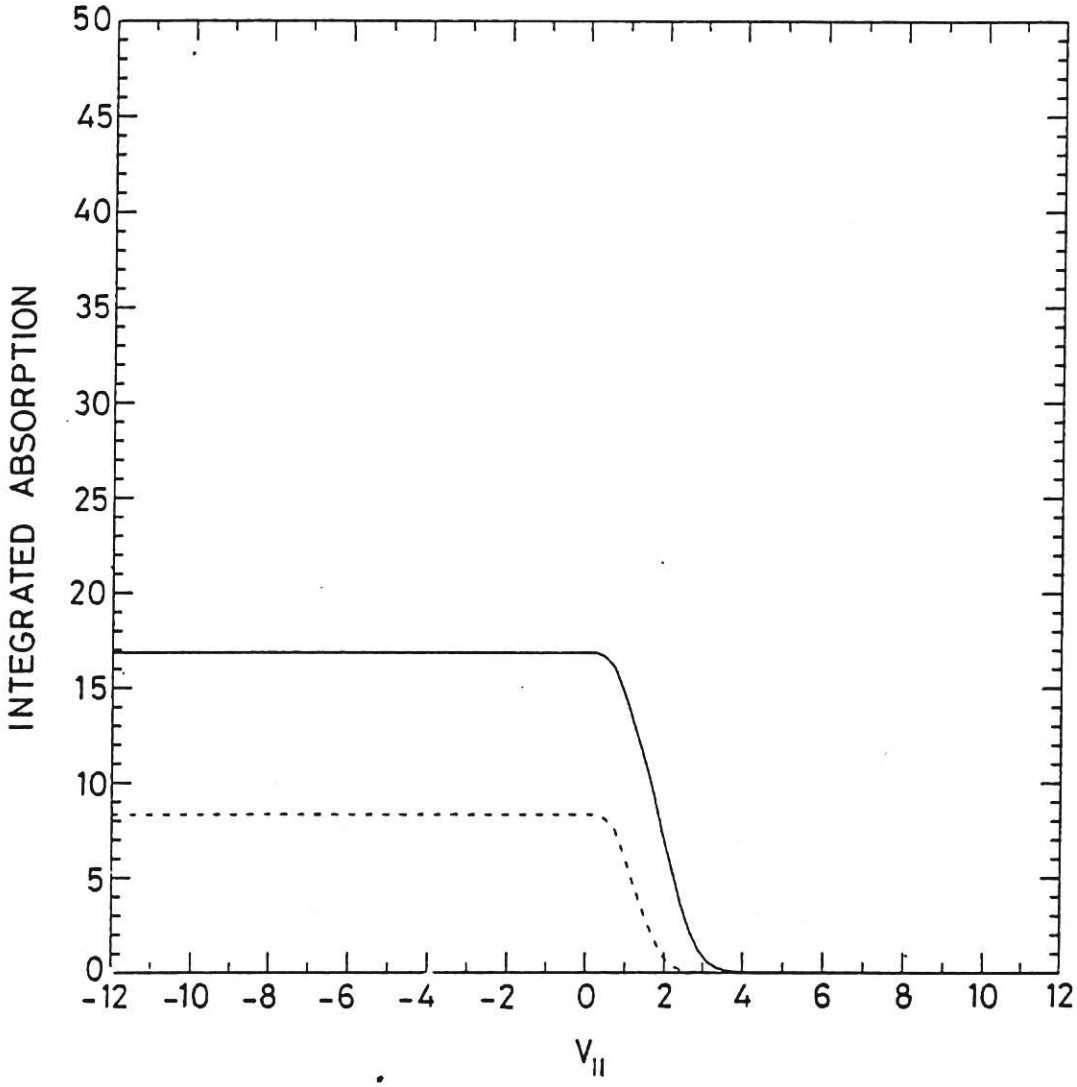

Fig. 9 Integrated power deposition as a function of parallel electron velocity, for parameters of Fig. 8.

CLM-P784